Published in final edited form as:
Ultrasound Med Biol. 2014 February ; 40(2): 400–409. doi:10.1016/j.ultrasmedbio.2013.09.024.

Synthesis and characterization of transiently stable albumin-coated microbubbles via a flow-focusing microfluidic device

Johnny L. Chen[a], **Ali H. Dhanaliwala**[a], **Adam J. Dixon**[a], **Alexander L. Klibanov**[b], and **John A. Hossack**[a,*]

[a]Department of Biomedical Engineering, University of Virginia, Charlottesville, Virginia, USA

[b]Department of Medicine - Cardiovascular Division, University of Virginia, Charlottesville, Virginia, USA

Abstract

We present a method of synthesizing albumin-shelled, large diameter (>10 μm), transiently-stable microbubbles using a flow-focusing microfluidic device (FFMD). Microfluidic device production enables microbubbles to be produced immediately prior to insonation, thus relaxing the requirements for stability. Both reconstituted fractionated bovine serum albumin (BSA) and fresh bovine blood plasma were investigated as shell stabilizers. Microbubble coalescence was inhibited by the addition of either dextrose or glycerol and propylene glycol. Microbubbles were observed to have an acoustic half-life of approximately 6 s. Microbubbles generated directly within a vessel phantom containing flowing blood produced a 6.5 dB increase in acoustic signal within the lumen. Microbubbles generated in real-time upstream of *in vitro* rat aortic smooth muscle cells under physiological flow conditions successfully permeabilized 58 % of the cells upon insonation at a peak negative pressure of 200 kPa. These results demonstrate that transiently-stable microbubbles produced via flow-focusing microfluidic devices are capable of image enhancement and drug delivery. In addition, successful microbubble production with blood plasma suggests the potential to utilize blood as a stabilizing shell.

Keywords

Flow-focusing microfluidic device; monodisperse microbubbles; albumin shell; ultrasound-mediated drug delivery; sonoporation

Introduction

Size distribution and stability are two important considerations for any microbubble formulation. Size is important as it dictates the acoustic properties of microbubbles. Microbubbles less than 1 μm in diameter produce minimal acoustic contrast (Soetanto and Chan, 2000; Gorce et al., 2000). Larger microbubbles provide increased contrast (Streeter et al., 2010; Kaya et al., 2010), but as microbubbles exceed 10 μm, they quickly get filtered by the lungs and can pose an emboli risk (Butler and Hills, 1979; Klibanov, 2002). Microbubble size has also been shown to affect drug delivery (Konofagou et al., 2012;

*Corresponding Author: John A Hossack, PO Box 800759 Charlottesville, VA 22908; jh7fj@virginia.edu; Phone: 434-243-5866.

Burke et al., 2012). Fan et al. (2012) recently demonstrated that cell membrane pore size following sonoporation increases with microbubble size and that different acoustic pressures can be used to selectively porate cells in contact with different sized microbubbles. Consequently, microbubbles are often size-sorted to reduce polydispersity or select a specific microbubble size (Kvåle et al., 1996; Huh et al., 2007; Feshitan et al., 2009; Borrelli et al., 2012). While narrow size distributions are attainable through sorting methods, microbubble yield is reduced and specific microbubble diameters are difficult to isolate from a polydisperse population.

Stability is important as it determines how well microbubbles survive the rigors of systemic circulation. Microbubbles are lost during intravenous administration (Talu et al., 2008b), filtered by the lungs, liver and spleen (Butler and Hills, 1979; Lim et al., 2004; Iijima et al., 2006), and dissolve and coalesce due to the complex multi-gas environment of the vasculature (Kabalnov et al., 1998; Kwan and Borden, 2010). To increase stability, newer generation microbubbles are formulated with low solubility gases to reduce dissolution and are stabilized with protein, polymer, or lipid shells (Sirsi and Borden, 2009).

Even with control of the microbubble size during production and increased stability, the *in vivo* distribution and concentration of microbubbles becomes unknown after microbubble administration. To overcome these limitations, we propose a new paradigm in which microbubbles are produced *in situ* directly within the vasculature, thus enabling controlled administration of microbubbles and therapeutics. Furthermore, by producing microbubbles in the vasculature near the target of interest, microbubbles can be intentionally designed to be unstable. As a result, larger microbubbles (> 10 μm), with their concomitant advantages, can be realized via transiently stable microbubbles that would mitigate the risk of emboli formation.

Flow-focusing microfluidic devices (FFMDs) are ideal for this application as they can produce monodisperse populations of microbubbles in real-time (Garstecki et al., 2004; Tan et al., 2006; Hettiarachchi et al., 2007; Wang et al., 2013) and can be miniaturized to be compatible with vasculature dimensions (Dhanaliwala et al., 2013). In addition, FFMDs are capable of producing microbubbles in sufficient quantities to provide acoustic contrast (Dhanaliwala et al., 2013) and facilitate drug delivery (Dixon et al., 2013) without the need for additional concentration or washing of the microbubbles prior to use. The ability to produce a monodisperse population of microbubbles at a specific microbubble diameter and concentration has implications for both imaging and drug delivery applications. Talu et al. (2007) observed that monodisperse microbubbles have reduced echo to echo decorrelation which could improve signal intensity, while Choi et al. (2010) observed that blood brain barrier penetration was improved when using 5 μm diameter compared to 1 μm diameter microbubbles.

Albumin has been extensively evaluated as a stabilizing shell material for ultrasound microbubble contrast agents (Keller et al., 1989; Ferrara et al., 2007; Sirsi and Borden, 2009), and it continues to be a relevant material because of its excellent safety profile (Vincent et al., 2003). In order to form a stable shell, albumin is typically heated in order to denature and cross-link the protein (Grinstaff and Suslick, 1991). While non-cross-linked albumin can be used as a microbubble shell, these microbubbles have a higher liquid-vapor surface tension (i.e. Laplace pressure) (Krishnan et al., 2004) and thus lower stability compared to cross-linked albumin-shelled microbubbles (Grinstaff and Suslick, 1991; Avivi and Gedanken, 2002). Albumin cross-linking can be difficult to achieve within an FFMD. As a result, there has been minimal investigation into albumin stabilized microfluidic produced microbubbles. However, for *in situ* microbubble production, a non-cross linked albumin shell could provide both biocompatibility and transient-stability.

In this study, we demonstrate *in vitro* production and characterization of transiently-stable microbubbles from an FFMD as a step towards the goal of *in situ* microbubble production. Nitrogen-filled albumin-coated microbubbles from an FFMD using both fractionated bovine serum albumin (BSA) and fresh bovine plasma were fabricated. The FFMD was characterized for microbubble diameter, production, and coalescence. Microbubble stability was characterized optically and acoustically. Finally, acoustic contrast of the microbubbles in a flow phantom and microbubble-enhanced drug delivery to an *in vitro* cell monolayer under physiological flow conditions were investigated.

Materials and Methods

FFMD Fabrication

Flow-focusing microfluidic devices (FFMDs) were fabricated as described previously (Dhanaliwala et al., 2013). Briefly, microfluidic devices were cast in polydimethylsiloxane (PDMS) (Sylgard 184, Dow Corning Corp., Midland, MI) from a custom SU-8 mold. The device was then plasma bonded to a clean PDMS substrate and heated at 70°C for 1 hour prior to use to ensure hydrophobicity of the channels. The final dimensions of the gas and liquid channels were 35 and 50 μm wide, respectively, the nozzle was 7 μm wide, and all channels were 27 μm tall.

Microbubble Fabrication

The liquid phase consisted of 3 or 5 % (w/v) bovine serum albumin (BSA) dissolved in a solution of isotonic saline (0.9 % NaCl) or a solution of glycerol, propylene glycol, and isotonic saline (GPS). Dextrose was added to either solution as needed. All chemicals were purchased from Sigma-Aldrich (St. Louis, MO). A pharmaceutical grade preparation of 5 % human serum albumin (HSA) (BSL Behring, King of Prussia, PA) was also tested. Albumin concentration was determined by absorbance at 280 nm (NanoDrop 1000, Thermo Scientific, Wilmington, DE) assuming a molar extinction coefficient of 6.7 M^{-1} cm^{-1}. Viscosity (η) was measured with an Ubbelohde viscometer (Cannon Instrument Company, State College, PA) at 23°C. The gas phase consisted of 99.998 % nitrogen (GTS Welco, Richmond, VA). PTFE tubing (Cole Parmer Vernon Hills, IL) 30 cm in length was used to convey the liquid and gas phase to the microfluidic device inlets. The liquid flow rate was set with a syringe pump (PHD Ultra, Harvard Apparatus, Holliston, MA) and the gas pressure was set with a two-stage pressure regulator (VTS 450D, Victor Technologies International, Inc., St. Louis, MO).

Microbubble Characterization

Microbubbles generated from the FFMD were characterized for production rate, diameter, and coalescence by analyzing images at the orifice and 1.7 mm downstream of the orifice. A high speed camera (SIMD24, Specialised Imaging, Tring, United Kingdom) was used to acquire the images. A high frame rate (2×10^6 frames per second (fps)) was required in order to adequately resolve microbubble formation at the orifice as production rates could reach 600,000 microbubbles/s (MB/s). Any microbubble resulting from the fusion of two or more microbubbles was considered a coalesced microbubble. Microbubble production rate and diameter were calculated from the images using ImageJ (NIH, Bethesda, MD). Monodispersity was defined as a polydispersity index (standard deviation/mean × 100 %) less than 10 %.

Microbubble stability was estimated optically and acoustically. In the optical method, microbubbles were collected at room temperature (23°C) under a glass slide as they were produced by the FFMD. Videos of the microbubbles over time were then taken with a digital camera (Canon T3i, Canon, Lake Success, NY). Every 100th frame was analyzed and the

number of microbubbles with diameters between 4–38 μm was counted using a custom circular Hough transform algorithm (Ballard, 1981) developed in Matlab (Mathworks, Natick, MA). The lower limit was selected based on the optical resolution of the images. The upper limit was selected to be double the largest microbubble expected to be produced. The microbubble optical half-life (T_{mb}) was defined as the time until half the maximum number of microbubbles remained in the field of view. In the acoustic method, a temperature controlled (16, 23, 37°C) solution of deionized (DI) water and microbubbles was continuously mixed and imaged with a Siemens Sequoia 512 clinical scanner (15L8 transducer, Siemens Medical Solutions, Malvern, PA). A contrast agent specific nonlinear imaging mode (Contrast Pulse Sequence [CPS] (Phillips, 2001)) at a center frequency of 7 MHz and mechanical index (MI) of 0.2 was used to minimize ultrasound destruction of microbubbles. An FFMD producing microbubbles was placed in the beaker until the ultrasound image intensity was saturated, after which the FFMD was removed. The image intensity over time was analyzed in Matlab by averaging a 30 × 30 pixel window in each frame. Each time-intensity curve was aligned by peak intensity and averaged ($n \geq 5$). The microbubble acoustic half-life (T_i) was calculated as the time until half the maximum intensity.

Cell Culture and Calcein Delivery

Primary rat aortic smooth muscle cells were cultured and plated on Thermanox coverslips (Nunc, Rocherster, NY) as previously described (Dixon et al., 2013). After the cells reached confluency, the coverslips were placed in a flow chamber designed to maintain laminar flow over the cells. A peristaltic pump (Wheaton Science Products, Millville, NJ) was used to pull 37°C phosphate buffered saline with calcium and magnesium (PBS +/+, Fisher Scientific) through the flow chamber at an average flow rate of 9 mL/s. The FFMD was placed inside the custom flow chamber and operated to produce 11 μm diameter microbubbles at a rate of 660,000 MB/s. Calcein (Sigma-Aldrich), a membrane impermeable fluorophore (Ex/Em 495/515 nm), was co-delivered with the microbubbles from a PTFE tube affixed next to the microbubble outlet. The calcein was supplied at a flow rate that gave a final concentration of 0.05 mg/mL within the flow chamber.

Only the effect of ultrasound peak negative pressure (PNP) on drug delivery was investigated. An ultrasound center frequency of 500 kHz (V301 Olympus Panametrics, Waltham, MA) was selected to best match the resonant frequency of the microbubbles (de Jong et al., 2002), and all pulses were 30 cycles long with a pulse repetition frequency (PRF) of 100 Hz. PNPs of 0, 100, 200, 300 kPa were investigated. Ultrasound was applied for two minutes while microbubbles and calcein flowed through the flow chamber. After the insonation period, the FFMD was removed from the flow chamber and flow was maintained for a few additional seconds to clear residual microbubbles and calcein from the channel. Flow was then stopped and the cells were allowed to rest for 2 minutes before being transferred to a petri dish and counter-stained with propidium iodide (PI) (MP Biomedicals, Santa Ana, CA), a marker of cell death, at a concentration of 25 μg/mL for 30 minutes at 37°C. The cells were imaged using fluorescence microscopy within 6 hours of PI staining.

Plasma Microbubbles

Bovine blood from an FDA approved abattoir was collected in 1.86 mg/mL ethylenediaminetetraacetic acid (EDTA). The plasma was separated from the blood by centrifugation at 500g for 30 min at 20°C to obtain a clear orange/pink supernatant. Glycerol and propylene glycol were added to the plasma at a volume concentration of 2.5 % each (2.5 % GP). Large aggregates and remaining red blood cells were filtered out using 8 and 2.5 μm pore-size filter paper (Grade 2, 5, Whatman, Maidstone, ME) followed by 0.45 μm pore

syringe filters (Fisher Scientific, Waltham, MA). The plasma solution was used within 7 days of collection and was supplied to the FFMD as described above.

Plasma microbubbles were imaged in a gelatin flow phantom — 6 % (w/v) gelatin (Type B, Fisher Scientific) and 1 % (w/v) Agar (Fisher Scientific) — with a 4 mm diameter lumen to simulate contrast enhancement in a blood vessel (Fig 5a). A FFMD producing 16 μm diameter plasma stabilized microbubbles at a rate of 125,000 MB/s was placed in 100 mL of bovine blood under constant agitation. The blood and microbubbles were pulled through the flow phantom at a flow rate of 105 mL/min (velocity ≈ 0.14 m/s) using a syringe pump. Microbubbles were imaged with the Sequoia 512 (CPS mode, center frequency = 7 MHz, MI = 0.2) and contrast to noise (CNR) was measured within a 30 × 30 pixel window in the lumen as:

$$CNR = 20\log_{10}\left(\frac{\mu_\omega - \mu_{\omega o}}{\sigma_{\omega o}}\right), \quad (1)$$

where μ_{wo} and σ_{wo} are the mean and standard deviation of pixel intensity without microbubbles and μ_w is the mean pixel intensity with microbubbles. Microbubble stability was measured in the flow phantom by stopping microfluidic production and flow, and measuring T_i. Ultrasonic destruction of microbubbles was investigated by stopping flow, increasing the MI to 1.9, and measuring T_i.

Statistical Analysis

In all cases, Student t-tests were used to determine statistical significance between experimental conditions. A p-value less than 0.05 was considered to be significant. For BSA microbubble stability studies, at least five trials were conducted for the acoustic and optical determinations. For the bovine plasma microbubbles in blood, stability and destruction was analyzed by conducting four trials each at an MI = 0.2 or 1.9.

For calcein delivery, each pressure condition was investigated in triplicate. The number of cells that internalized calcein and the number of nuclei stained with PI in each image were counted. Percentages were calculated using the total number of cells prior to insonation, as ultrasound can cause cells to dislodge *in vitro* (Liu et al., 2012). Cell dislodgement was calculated as the percent difference between the cells remaining on the insonated coverslip and the number of cells on the control coverslip.

Results

Albumin Microbubble Production and Coalesence

By applying gas pressures and liquid flow rates between 48.3–68.9 kPa and 50–80 μL/min, respectively, microbubbles with diameters between 10–20 μm at rates between 1–6 × 10^5 MB/s could be produced. At these high production rates, however, microbubbles stabilized with BSA alone were observed to coalesce. The microbubbles would have a uniform diameter at the nozzle but would then coalesce downstream, resulting in a polydisperse size distribution (Fig 1d). At a constant concentration of 10 % (w/v) dextrose, BSA concentrations greater than 3 % prevented coalescence (Fig 1a,e). At a constant concentration of 3 % BSA, dextrose concentrations greater than 5 %) eliminated coalescence. For GPS, however, only a concentration of 2.5 % glycerol, 2.5 % propylene glycol, and 95 % (v/v) saline (2.5 % GPS) was observed to eliminate coalescence (Fig 1b,c). Similarly, for microbubbles stabilized with 5 % HSA, dextrose at concentrations greater than 5 % eliminated coalescence. A solution of only 10 % dextrose in saline or 2.5 % GPS or both failed to produce stable microbubbles. A solution of 3 % BSA had a viscosity of

1.10 mP s. Adding 2.5 % GPS increased the viscosity to 1.28 mP s, while adding 10 % dextrose increased the viscosity to 1.42 mP s. All further experiments were conducted with optimized solutions of 3 % BSA with 10 % dextrose (BSA-DEX) or 3 % BSA and 2.5 % GPS (BSA-GPS).

BSA Microbubble Stability

For the optical method, the microbubbles were measured to be initially 12 μm in diameter and monodisperse before undergoing Ostwald ripening (Talu et al., 2008a). Shrinking microbubbles disappeared while microbubbles that grew persisted for the duration of the observation (2 min) (Fig 2). The T_{mb} of microbubbles fabricated from BSA-DEX or BSA-GPS at 23°C were 27.0 ± 5.3 s and 26.9 ± 5.4 s, respectively (Fig 2). There was no statistically significant difference between the two formulations.

For the acoustic method, the microbubbles were measured to be 13 μm in diameter before being placed in the beaker. The T_i at 23°C was measured to be 6.8 ± 1.9 s and 6.6 ± 2.2 s for microbubbles stabilized with BSA-GPS or BSA-DEX, respectively. The T_i determined at 16°C was statistically different ($p < 0.05$) from 23°C and 37°C for the respective formulations (Fig 3). There was no statistically significant difference between the two formulations at each respective temperature.

Calcein Delivery

There was no significant cell dislodgement at a flow rate of 9 mL/s (velocity ≈ 0.19 m/s, wall shear stress ≈ 0.24 mN/cm^2) in the absence of ultrasound and microbubbles. No calcein uptake was observed when either ultrasound or microbubbles were applied alone. Significantly enhanced calcein delivery was observed at PNPs of 200 and 300 kPa (Fig 4c,d). The maximum cell permeabilization achieved was 58 % at an insonation pressure of 200 kPa, while a maximum cell death of 14 % was observed at 300 kPa. Cell dislodgement was 1 %, 12 %, and 28 % at PNPs of 100, 200, 300 kPa, respectively.

Bovine Plasma Microbubbles

Production characteristics of bovine plasma microbubbles were similar to BSA microbubbles – greater than 10^5 MB/s for 10–16 μm diameter microbubbles. Blood plasma alone produced microbubbles that quickly coalesced. Adding dextrose up to 40 % reduced coalescence to less than 10 %, while 2.5 % GP eliminated coalescence. Microbubbles exited monodisperse (Fig 5b) and underwent Ostwald ripening, as with the BSA microbubbles, with more than 90 % of microbubbles dissolved after one minute.

The CNR of the gelatin phantom lumen in the presence of plasma-stabilized microbubbles was measured to be 15.4 dB (Fig 5c). At an MI of 0.2, T_i was calculated to be 3.2 ± 0.2 s. At an MI of 1.9, T_i was found to be shorter at 0.9 ± 0.4 s ($p < 0.0001$) (Fig 5d)).

Discussion

Microbubble coalescence and stability

A solution of BSA with either GPS or dextrose prevented microbubble coalescence (Fig 1b,c). In addition, no significant difference in microbubble stability—either optically or acoustically—was found between formulations (Fig 2,Fig 3). Bulk liquid viscosity has been found to both prevent microbubble coalescence by increasing the coalescence time (Sanada et al., 2005; Talu et al., 2006) and facilitate coalescence by increasing the interaction between microbubbles (Chen et al., 1998). Thus, these two opposing effects may explain the optimum GPS concentration (2.5 %) that was necessary to form stable albumin-coated microbubbles. Dextrose has also been shown to stabilize sonicated albumin microbubbles,

resulting in longer contrast duration (Porter et al., 1994) or increased therapeutic delivery (Browning et al., 2012). The mechanism behind these observations has not been entirely elucidated. Browning et al. (2012) suggest that dextrose may be glycating albumin, leading to a more stable shell. In our experiments there were no detectable difference from mass spectroscopy of samples of BSA and BSA-DEX (data not shown). Since there was no heating step in our microfluidic system, it is unlikely that glycation is primarily responsible for stabilizing the shell. Instead, dextrose may have the same viscosity effect as GPS. Alternatively, dextrose may stabilize the shell by initially adsorbing on the surface of nascent microbubbles, preventing coalescence until the larger albumin can adsorb onto the microbubble. More studies, however, are needed to elucidate the exact mechanism.

To more closely approximate the environment of blood found *in vivo*, microbubble lifetimes were evaluated in air-saturated media. All solutions were well-mixed and none of the solutions were degassed. Gas content was not monitored specifically, but solutions were assumed to be saturated with room air. When measured optically, microbubble half-life was observed to be longer than when measured acoustically (i.e. $T_{mb} > T_i$). Optically, microbubbles were observed to shrink; however, this would not affect T_{mb} until the diameter falls below 4 μm. On the other hand, acoustic signal loss due to microbubble shrinkage would be captured by the acoustic method and lead to a shorter T_i. Furthermore, in the optical method the microbubbles were static, while in the acoustic method the microbubbles were under constant agitation. This agitation may have accelerated microbubble dissolution and thus shortened T_i. Since only the acoustic response is imaged *in vivo*, we believe the acoustic half-life (T_i) to be a more practical indication of microbubble stability. Using the acoustic method, it was also observed that T_i was reduced at 16°C as compared to 23 and 37°C (Fig 3). This is likely a consequence of the increased gas solubility that occurs with decreasing temperature.

Since neither heat nor sonication was used, it is unlikely that there was significant cross-linking between albumin molecules. Thus, weaker non-covalent forces (hydrogen bonds and hydrophobic interactions) may primarily be responsible for the formation of the shell (Hellebust et al., 1993), and resulting in rapid microbubble dissolution. While unstable microbubbles may not be useful for systemic administration, low stability is advantageous when using larger microbubbles as it would enhance microbubble dissolution and potentially minimize the risk of gas emboli formation.

Drug Delivery

Albumin-stabilized microbubbles successfully enhanced calcein uptake by smooth muscle cells despite their transient stability, suggesting that long-lived microbubbles are not necessary to effect drug delivery. A clear threshold for delivery between 100 kPa and 200 kPa (Fig 4e) was observed, suggesting that ultrasound parameters and microbubble production rate must be optimized to maximize delivery and minimize cell death. Maximum cell dislodgement was observed at a PNP of 300 kPa. At this pressure, microbubbles were observed to aggregate on the Thermanox coverslips, possibly due to increased secondary radiation force (Dayton et al., 1999). This increased local microbubble concentration may have caused greater cell dislodgement and acoustic attenuation, and thus reduced cell permeabilization and delivery. Cell dislodgement, however, is probably exaggerated *in vitro*, as compared to *in vivo*, due to the lack of a basement membrane and other anchoring proteins.

Local microbubble concentration is highly variable depending on factors such as injection site, method of administration (e.g. infusion or bolus), and transit time (i.e. distance to location of interest). By using a microfluidic platform, microbubble concentration—and thus the therapeutic efficacy—can be more precisely controlled. Microbubble size and

composition could be tailored for specific applications, predefined or in real-time, and a therapeutic agent could be co-injected, as in our study, or incorporated directly in the liquid phase (Peyman et al., 2012).

We envisage integrating the microfluidic platform with an IVUS catheter to enable local microbubble production and insonation. While most IVUS transducers are designed for frequencies greater than 10 MHz, Kilroy and Hossack (2011) have fabricated an IVUS transducer capable of achieving 600 kPa at 1.5 MHz by operating the transducer in a width mode. Furthermore, capacitive micro-machined ultrasonic transducers (CMUTs) have the potential to enable production of low frequency transducers with IVUS compatible dimensions (Certon et al., 2013). As a result, it may be possible to fabricate IVUS transducers capable of emitting frequencies better matched to the lower resonant frequency of larger diameter microbubbles.

Plasma Microbubbles

Optimizing albumin as a shell material is a step towards using a patient's own blood to produce microbubbles. By utilizing the albumin from blood plasma, the small risk of an immune response to the microbubble shell could be further reduced, if not eliminated. In addition, plasma could be obtained from the patient immediately prior to microbubble fabrication, eliminating the need for storage. Plasma would also be an ideal stabilizer for microbubbles produced directly into the vasculature since the excess plasma is inherently biocompatible and need not be washed away.

Microbubbles were successfully fabricated from bovine blood plasma with the addition of 2.5 % GPS. The addition of dextrose reduced but failed to completely eliminate coalescence. These results suggest that dissimilar mechanisms act to stabilize the microbubble shell; however, more studies are needed to evaluate the effects of other surface active components (e.g. proteins, clotting factors, lipids, etc.) in blood plasma that may have contribute to microbubble stabilization. The plasma microbubbles stabilized with GP exhibited similar production characteristics to BSA microbubbles. The microbubbles were fabricated as a monodisperse population then quickly dissolved. No insoluble aggregates were optically resolvable at 40× magnification, suggesting that the shell solubilizes when the microbubbles shrink and collapse. The plasma microbubbles, however, exhibited a shorter T_i as compared to BSA-stabilized microbubbles. The T_i was further reduced when the MI was increased to 1.9. Consequently, other molecules in the plasma may be interfering with the ability of albumin to adequately stabilize the microbubble.

Finally, we observed that plasma microbubbles produced at rates as low as 10^5 MB/s were capable of providing sufficient acoustic (Fig 5c). Traditionally, microbubbles are administered on the order of 10^9 microbubbles per patient (Lantheus Medical (2008); GE Healthcare (2012)). An FFMD operating at 10^5 MB/s would require 2.75 hours to achieve a similar dose. However, by locally producing microbubbles, we were able to provide the necessary contrast with only a few seconds of microbubble production. While additional studies are necessary to compare the acoustic signal from equivalent concentrations of current generation microbubbles and FFMD-produced microbubbles, these results suggest that if FFMDs are used to produce microbubbles locally, they do not need to achieve high microbubble production rates (i.e. > 10^6 MB/s).

Microbubble size

To date, smaller microbubbles have been utilized in order to minimize the risk of emboli formation. This is especially relevant for newer generation microbubbles composed of fluorocarbon gas, which are known to grow in size upon exposure to air saturated solutions

such as blood (Kabalnov et al., 1998; Talu et al., 2008a; Dixon et al., 2013). Scattering cross-section, however, increases with the sixth-power of microbubble radius (Medwin, 1977; Palma and Bertolotto, 1999) and microbubbles produce harmonics relative to the insonation frequency in addition to any arising from microbubble resonance effects. Thus, larger microbubbles have an increased acoustic signal at all clinically relevant ultrasound frequencies as compared to smaller microbubbles, even when smaller microbubbles are insonated at resonance (Streeter et al., 2010). Larger microbubbles have also been shown to have increased bio-effects that can be utilized for sonoporation (Choi et al., 2010; Fan et al., 2012). Consequently, by intentionally producing transiently-stable microbubbles, the advantages of larger microbubbles can be utilized without the increased risk of emboli formation.

Limitations

The focus of the present study was to investigate and characterize albumin-stabilized microbubbles produced via an FFMD. While the ultimate goal is to develop the paradigm of *in situ* microbubble production, we chose to use an FFMD with non-vascular compatible dimensions as these devices provide larger imaging windows through which the microbubbles can be optically characterized. Similarly, an FFMD placed at the tip of a catheter would require the gas input tubing to be greater than 130 cm in length in order to extend the length of the catheter. We chose to use shorter tubing in order to focus on microbubble characterization. Consequently, the effect of device size and input tubing length on FFMD operation and microbubble production requires additional study.

To maximize the cell-to-microbubble ratio during drug delivery, the FFMD was operated near its maximum production rate. On the other hand, for imaging, the FFMD was operated at a lower production rate to minimize acoustic signal saturation. A thorough analysis on the effect of microbubble production rate on drug delivery and image enhancement was not performed, however, and additional studies are needed to determine the optimal production rate for each of these situations.

As our goal was only to verify that plasma-stabilized microbubbles could be successfully imaged within blood, we did not compare the acoustic signal with that from traditional albumin microbubbles such as Optison (GE Healthcare). Using an optimized and consistent set of imaging parameters will enable future studies to compare the acoustic signal from multiple microbubble contrast agent formulations across multiple imaging studies.

Because of inter-device variation with current fabrication methods, a specific set of gas and liquid input parameters does not always result in exactly the same microbubble diameter and production rate for a given FFMD. However, once an FFMD has been characterized and calibrated, the resulting microbubble diameter and production rate for a given set of gas and liquid input parameters are within 10 % of their expected values. Furthermore, while we can optically confirm microbubble diameter and production rate before and after, we currently cannot directly confirm microbubble properties during an ultrasound imaging or drug delivery procedure.

Conclusions

We report the first case of microbubbles generated using a flow-focusing microfluidic device but stabilized with fractionated BSA or blood plasma. Microbubbles stabilized with albumin alone coalesce within the microfluidic device. The addition of either dextrose or glycerol plus propylene glycol, however, eliminates this behavior. Although the albumin-stabilized microbubbles exhibited short half-lives, it was sufficient to enhance acoustic contrast and enable sonoporation. Overall, the ability to produce microbubbles stabilized

with plasma is another step toward our goal of utilizing flow-focusing microfluidic devices for *in situ* microbubble production directly within the vasculature.

Acknowledgments

This work is funded in part by National Institutes of Health grant NHLBI R01 HL090700 to ALK, JAH. The high speed camera was funded by a shared instrumentation grant S10 RR025594 to JAH. AJD is supported by a NSF Graduate Research Fellowship and AHD is supported by an American Heart Association Graduate Fellowship. The content is solely the responsibility of the authors and does not necessarily represent the official views of the NIH or AHA. The authors would like to thank Gore Processing Inc (Edinburg, VA) for providing bovine blood.

References

Avivi S, Gedanken A. S-s bonds are not required for the sonochemical formation of proteinaceous microspheres: the case of streptavidin. The Bio-chemical journal. 2002; 366(Pt 3):705–707.

Ballard D. Generalizing the hough transform to detect arbitrary shapes. Pattern Recognition. 1981; 132:111–122. WOS:A1981LH42300002.

Borrelli MJ, O'Brien William DJ, Bernock LJ, Williams HR, Hamilton E, Wu J, Oelze ML, Culp WC. Production of uniformly sized serum albumin and dextrose microbubbles. Ultrasonics sonochemistry. 2012; 191:198–208. [PubMed: 21689961]

Browning RJ, Mulvana H, Tang MX, Hajnal JV, Wells DJ, Eckersley RJ. Effect of albumin and dextrose concentration on ultrasound and microbubble mediated gene transfection in vivo. Ultrasound in medicine & biology. 2012; 386:1067–1077. [PubMed: 22502878]

Burke CW, Suk JS, Kim AJ, Hsiang YHJ, Klibanov AL, Hanes J, Price RJ. Markedly enhanced skeletal muscle transfection achieved by the ultrasound-targeted delivery of non-viral gene nanocarriers with microbubbles. Journal of controlled release: official journal of the Controlled Release Society. 2012; 1622:414–421. [PubMed: 22800583]

Butler BD, Hills BA. The lung as a filter for microbubbles. Journal of applied physiology: respiratory, environmental and exercise physiology. 1979; 473:537–543.

Certon D, Ternifi R, Boulme A, Legros M, Minonzio JG, Talmant M, Patat F, Remenieras JP. Low frequency cMUT technology: Application to measurement of brain movement and assessment of bone quality. IRBM. 2013; 342:159–166.

Chen, L.; Li, Y.; Manasseh, R. The coalescence of bubbles-a numerical study. third international conference on multiphase; Third International Conference on Multiphase Flow; 1998. p. 8-12.

Choi JJ, Feshitan JA, Baseri B, Wang S, Tung YS, Borden MA, Konofagou EE. Microbubble-size dependence of focused ultrasound-induced blood-brain barrier opening in mice in vivo. IEEE transactions on bio-medical engineering. 2010; 571:145–154. [PubMed: 19846365]

Dayton P, Klibanov A, Brandenburger G, Ferrara K. Acoustic radiation force in vivo: a mechanism to assist targeting of microbubbles. Ultrasound in Medicine & Biology. 1999; 258:1195–1201. [PubMed: 10576262]

de Jong N, Bouakaz A, Frinking P. Basic acoustic properties of microbubbles. Echocardiography (Mount Kisco, NY). 2002; 193:229–240.

Dhanaliwala AH, Chen JL, Wang S, Hossack JA. Liquid flooded flow-focusing microfluidic device for in situ generation of monodisperse microbubbles. Microfluidics and Nanofluidics. 2013; 143-4:457–467. [PubMed: 23439786]

Dixon AJ, Dhanaliwala AH, Chen JL, Hossack JA. Enhanced intracellular delivery of a model drug using microbubbles produced by a microfluidic device. Ultrasound in Medicine & Biology. 2013; 397:1267–1276. [PubMed: 23643062]

Fan Z, Liu H, Mayer M, Deng CX. Spatiotemporally controlled single cell sonoporation. Proceedings of the National Academy of Sciences. 2012; 10941:16486–16491.

Ferrara K, Pollard R, Borden M. Ultrasound microbubble contrast agents: fundamentals and application to gene and drug delivery. Annual review of biomedical engineering. 2007; 9:415–447.

Feshitan JA, Chen CC, Kwan JJ, Borden MA. Microbubble size isolation by differential centrifugation. Journal of colloid and interface science. 2009; 3292:316–324. [PubMed: 18950786]

Garstecki P, Gitlin I, DiLuzio W, Whitesides GM, Kumacheva E, Stone HA. Formation of monodisperse bubbles in a microfluidic flow-focusing device. Applied Physics Letters. 2004; 8513:2649–2651.

GE Healthcare. Optison (package insert). 2012.

Gorce JM, Arditi M, Schneider M. Influence of bubble size distribution on the echogenicity of ultrasound contrast agents: a study of SonoVue. Investigative radiology. 2000; 3511:661–671. [PubMed: 11110302]

Grinstaff MW, Suslick KS. Air-filled proteinaceous microbubbles: synthesis of an echo-contrast agent. Proceedings of the National Academy of Sciences of the United States of America. 1991; 8817:7708–7710. [PubMed: 1652761]

Hellebust H, Christiansen C, Skotland T. Biochemical characterization of air-filled albumin microspheres. Biotechnology and applied biochemistry. 1993; 18(Pt 3):227–237. [PubMed: 8297503]

Hettiarachchi K, Talu E, Longo ML, Dayton PA, Lee AP. On-chip generation of microbubbles as a practical technology for manufacturing contrast agents for ultrasonic imaging. Lab on a Chip. 2007; 74:463–468. [PubMed: 17389962]

Huh D, Bahng JH, Ling Y, Wei HH, Kripfgans OD, Fowlkes JB, Grotberg JB, Takayama S. Gravity-driven microfluidic particle sorting device with hydrodynamic separation amplification. Analytical Chemistry. 2007; 794:1369–1376. [PubMed: 17297936]

Iijima H, Moriyasu F, Miyahara T, Yanagisawa K. Ultrasound contrast agent, levovist microbubbles are phagocytosed by kupffer cells-in vitro and in vivo studies. Hepatology research: the official journal of the Japan Society of Hepatology. 2006; 354:235–237. [PubMed: 16831566]

Kabalnov A, Klein D, Pelura T, Schutt E, Weers J. Dissolution of multicomponent microbubbles in the bloodstream: 1. theory. Ultrasound in Medicine & Biology. 1998; 245:739–749. [PubMed: 9695277]

Kaya M, Feingold S, Hettiarachchi K, Lee AP, Dayton PA. Acoustic responses of monodisperse lipid-encapsulated microbubble contrast agents produced by flow focusing. Bubble Science Engineering and Technology. 2010; 22:33–40. [PubMed: 21475641]

Keller MW, Glasheen W, Kaul S. Albunex: a safe and effective commercially produced agent for myocardial contrast echocardiography. Journal of the American Society of Echocardiography: official publication of the American Society of Echocardiography. 1989; 21:48–52. [PubMed: 2627424]

Kilroy, J.; Hossack, J. Triple function IVUS: diagnostic imaging, radiation force, and therapeutic for microbubble-based drug delivery. Ultrasonics Symposium (IUS), 2011 IEEE International; 2011. p. 2173-2176.

Klibanov, A. Ultrasound contrast agents: Development of the field and current status. In: Krause, W., editor. Contrast Agents II. Vol. 222 of Topics in Current Chemistry. Springer Berlin; Heidelberg: 2002. p. 73-106.

Konofagou EE, Tung YS, Choi J, Deffieux T, Baseri B, Vlachos F. Ultrasound-induced blood-brain barrier opening. Current pharmaceutical biotechnology. 2012; 137:1332–1345. [PubMed: 22201586]

Krishnan A, Sturgeon J, Siedlecki CA, Vogler EA. Scaled interfacial activity of proteins at the liquid-vapor interface. Journal of biomedical materials research Part A. 2004; 683:544–557. [PubMed: 14762935]

Kvåle S, Jakobsen HA, Asbjornsen OA, Omtveit T. Size fractionation of gas-filled microspheres by flotation. Separations Technology. 1996; 64:219–226.

Kwan JJ, Borden MA. Microbubble dissolution in a multigas environment. Langmuir: the ACS journal of surfaces and colloids. 2010; 269:6542–6548. [PubMed: 20067292]

Lantheus Medical. Definity (package insert). 2008

Lim AKP, Patel N, Eckersley RJ, Taylor-Robinson SD, Cosgrove DO, Blomley MJK. Evidence for spleen-specific uptake of a microbubble contrast agent: a quantitative study in healthy volunteers. Radiology. 2004; 2313:785–788. [PubMed: 15118114]

Liu Y, Yan J, Prausnitz MR. Can ultrasound enable efficient intracellular uptake of molecules? a retrospective literature review and analysis. Ultrasound in medicine & biology. 2012; 385:876–888. [PubMed: 22425381]

Medwin H. Counting bubbles acoustically: a review. Ultrasonics. 1977; 151:7–13.

Palma LD, Bertolotto M. Introduction to ultrasound contrast agents: physics overview. European Radiology. 1999; 93:S338–S342. [PubMed: 10602924]

Peyman SA, Abou-Saleh RH, McLaughlan JR, Ingram N, Johnson BRG, Critchley K, Freear S, Evans JA, Markham AF, Coletta PL, Evans SD. Expanding 3D geometry for enhanced on-chip microbubble production and single step formation of liposome modified microbubbles. Lab on a chip. 2012; 1221:4544–4552. [PubMed: 22968592]

Phillips, P. Contrast pulse sequences (CPS): imaging nonlinear microbubbles. IEEE Ultrasonics Symposium. Vol. 2; Atlanta, GA. 2001. p. 1739-1745.

Porter TR, Xie F, Anderson JR, Kricsfeld A, D'Sa A. Multifold sonicated dilutions of albumin with fifty percent dextrose improve left ventricular contrast videointensity after intravenous injection in human beings. Journal of the American Society of Echocardiography: official publication of the American Society of Echocardiography. 1994; 75:465–471. [PubMed: 7986543]

Sanada T, Watanabe M, Fukano T. Effects of viscosity on coalescence of a bubble upon impact with a free surface. Chemical Engineering Science. 2005; 6019:5372–5384.

Sirsi S, Borden M. Microbubble compositions, properties and biomedical applications. Bubble science engineering and technology. 2009; 11-2:3–17. [PubMed: 20574549]

Soetanto K, Chan M. Fundamental studies on contrast images from different-sized microbubbles: analytical and experimental studies. Ultrasound in Medicine & Biology. 2000; 261:81–91. [PubMed: 10687796]

Streeter JE, Gessner R, Miles I, Dayton PA. Improving sensitivity in ultrasound molecular imaging by tailoring contrast agent size distribution: in vivo studies. Molecular imaging. 2010; 92:87–95. [PubMed: 20236606]

Talu, E.; Hettiarachchi, K.; Nguyen, H.; Lee, A.; Powell, R.; Longo, M.; Dayton, P. P2A-8 lipid-stabilized monodisperse microbubbles produced by flow focusing for use as ultrasound contrast agents. IEEE Ultrasonics Symposium, 2006; Vancouver, BC, Canada. 2006. p. 1568-1571.

Talu E, Hettiarachchi K, Powell RL, Lee AP, Dayton PA, Longo ML. Maintaining monodispersity in a microbubble population formed by flow-focusing. Langmuir: the ACS journal of surfaces and colloids. 2008a; 245:1745–1749. [PubMed: 18205422]

Talu E, Hettiarachchi K, Zhao S, Powell RL, Lee AP, Longo ML, Dayton PA. Tailoring the size distribution of ultrasound contrast agents: possible method for improving sensitivity in molecular imaging. Molecular Imaging. 2007; 66:384–392. [PubMed: 18053409]

Talu E, Powell RL, Longo ML, Dayton PA. Needle size and injection rate impact microbubble contrast agent population. Ultrasound in Medicine & Biology. 2008b; 347:1182–1185. [PubMed: 18295967]

Tan YC, Cristini V, Lee AP. Monodispersed microfluidic droplet generation by shear focusing microfluidic device. Sensors and Actuators B: Chemical. 2006; 1141:350–356.

Vincent JL, Wilkes MM, Navickis RJ. Safety of human albumin–serious adverse events reported worldwide in 1998-2000. British journal of anaesthesia. 2003; 915:625–630. [PubMed: 14570782]

Wang S, Dhanaliwala AH, Chen JL, Hossack JA. Production rate and diameter analysis of spherical monodisperse microbubbles from two-dimensional, expanding-nozzle flow-focusing microfluidic devices. Biomicrofluidics. 2013; 71:014103–014103–12.

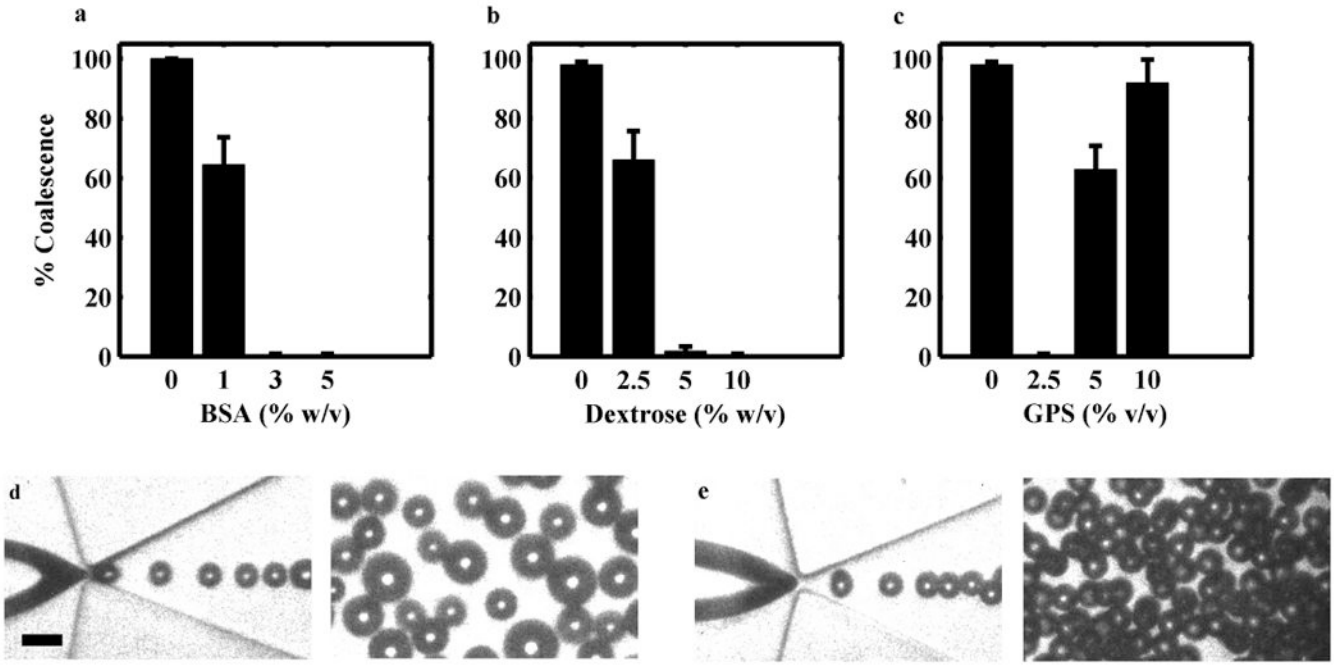

Figure 1.

Effect of BSA, dextrose and GPS concentration on microbubble coalescence. Microbubbles were imaged downstream of an FFMD operating at a gas pressure of 58.6 kPa. At a constant concentration of 10 % dextrose, (a) increasing BSA prevented coalescence. At a constant concentration of 3 % BSA, (b) increasing dextrose prevented coalescence, while (c) an optimal concentration of 2.5 % GPS was required to prevent coalescence. (Plotted as mean + one standard deviation, n = 3). Representative high-speed images of coalesced microbubbles (d) and stable monodisperse microbubbles (e) at the nozzle and downstream (scale bar = 20 μm)

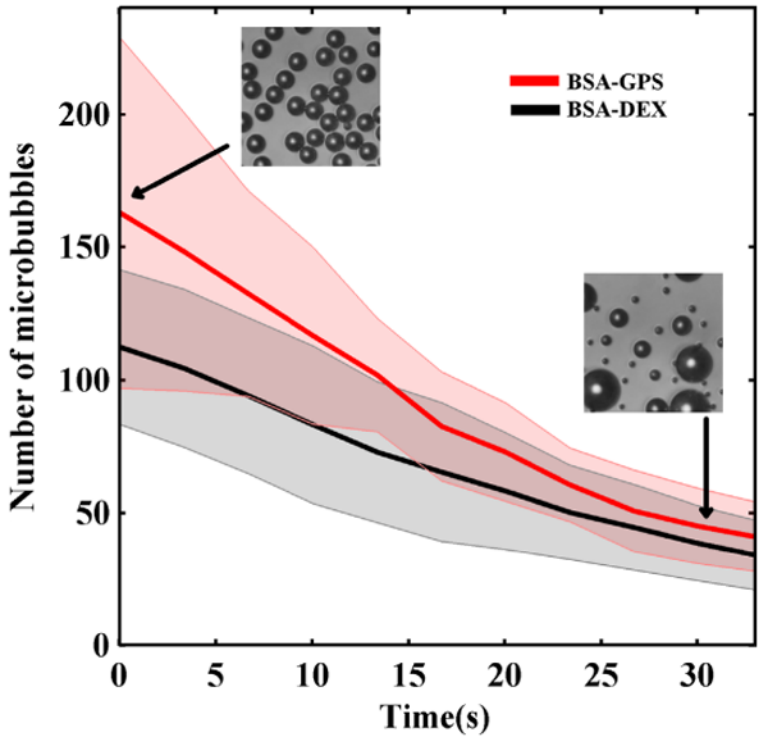

Figure 2.

Optical determination of microbubble half-life. No statistical significance in the time until half maximum number of microbubbles (T_{mb}) between BSA-DEX (T_{mb} = 27.0 ± 5.3 s) and BSA-GPS (T_{mb} = 26.9 ± 5.4 s) was observed. T_{mb} plotted as mean [solid] ± standard deviation [shaded], n = 6.

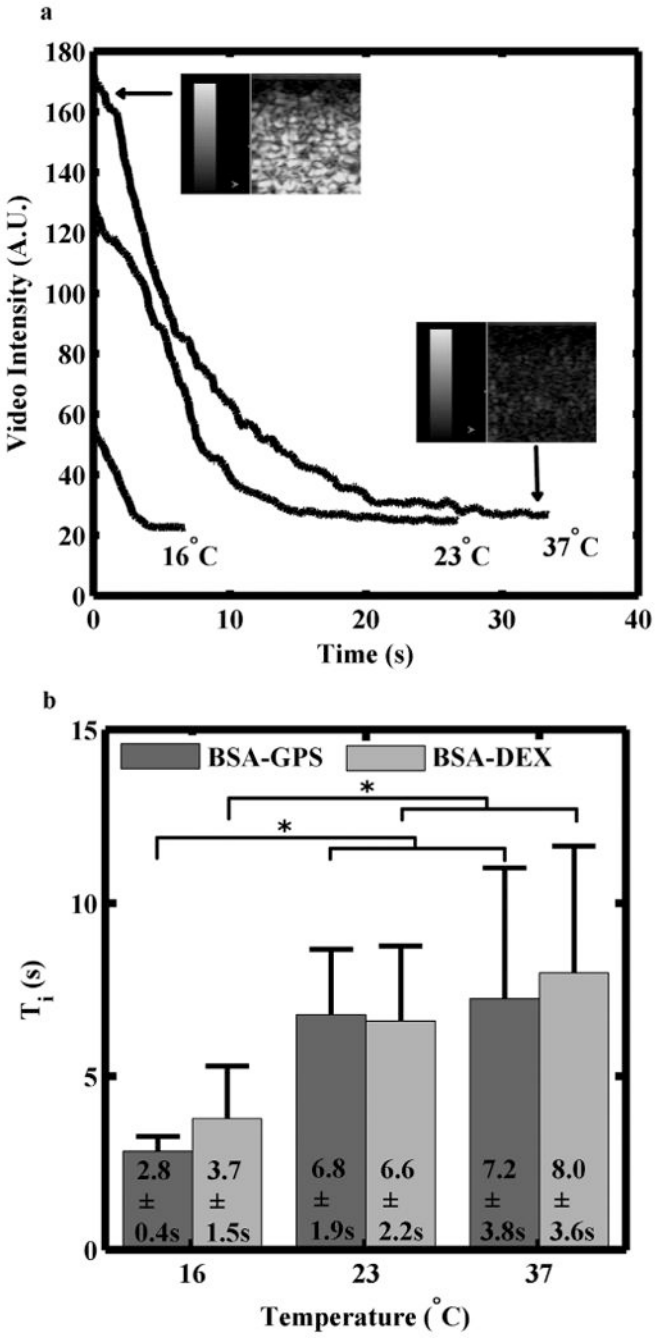

Figure 3.

Acoustic determination of microbubble half-life. (a) Microbubbles stabilized with either BSA-GPS or BSA-DEX showed similar rates of signal loss over time. (Dynamic range scale = 50 dB, and CPS gain = 0 dB). (b) No difference was observed in the time until half maximum image intensity (T_i) for the two formulations between 23°C and 37°C. Both formulations had a significantly lower T_i at 16°C. T_i plotted as mean + standard deviation, n ≥ 5, * = $p < 0.05$.

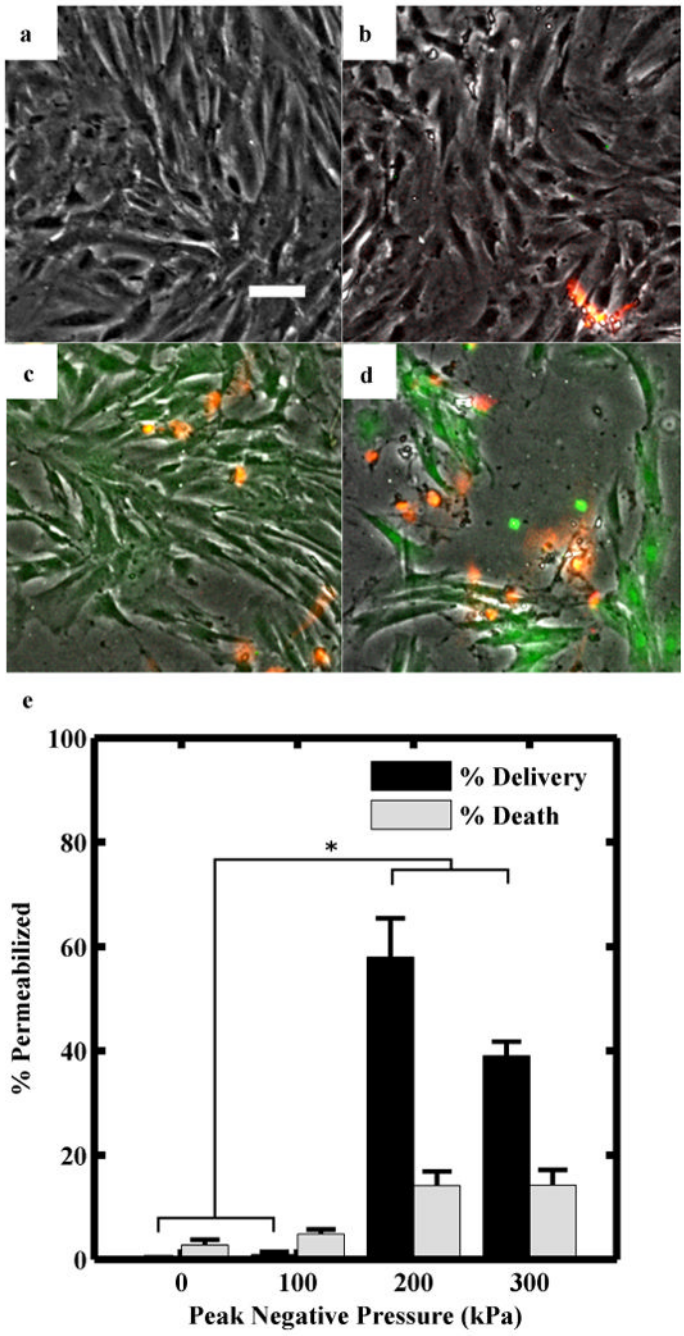

Figure 4.

(a-d) Representative fluorescence microscopy images of rat aortic smooth muscle cells following calcein delivery at peak negative pressures of 0, 100, 200, 300 kPa, respectively. Green fluorescence indicates calcein internalization; orange indicates cell death (scale bar = 50 μm). Flow rate was maintained at 9 mL/s. Microbubbles were 11 μm in diameter, composed of 3 % BSA, 2.5 % GPS, and nitrogen, and produced at a rate of 660,000 MB/s. (e) Calcein delivery and cell death at different ultrasound peak negative pressures. Percentages plotted as mean + one standard deviation, $n \geq 3$, * = $p < 0.0001$.

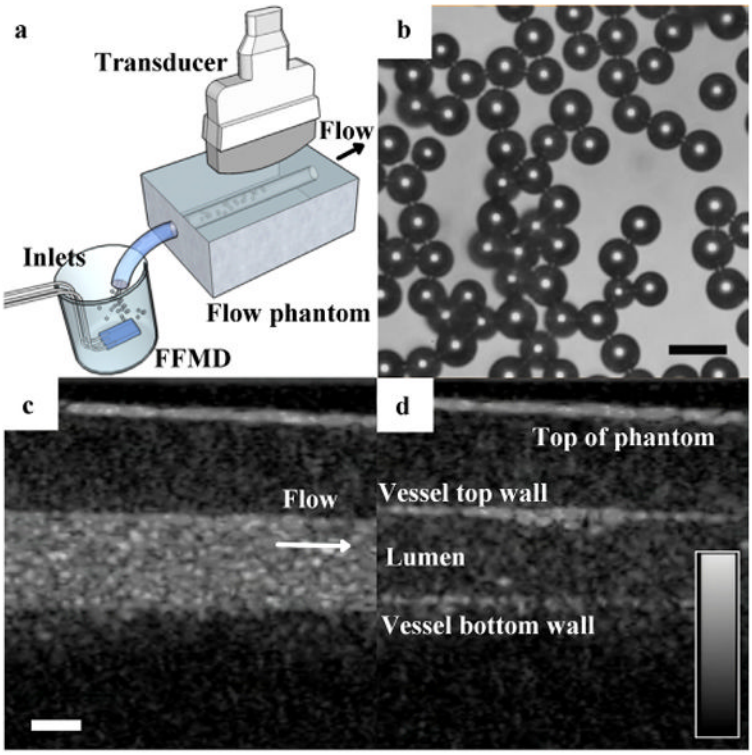

Figure 5.

(a) Microbubbles stabilized with bovine blood plasma were produced in whole bovine blood then drawn through a flow phantom and imaged. Arrow indicates flow direction. (b) Microbubbles immediately exiting the FFMD were monodisperse (polydispersity index < 10 %) (scale bar = 20 μm). (c) Microbubbles generated in real-time produced a CNR of 15.4 dB within the gelatin phantom vessel lumen. (d) Halting flow and increasing the MI to 1.9 resulted in microbubble destruction. (For bottom row: scale bar = 2 mm, dynamic range scale = 50 dB, CPS gain = 0 dB).